doi:10.3772/j.issn.1006-6748.2018.02.014

Effect of guide vane outlet angle on pump performance and impeller radial force in an axial-flow heart pump①

Liu Fufei(刘复飞)*, Sang Xiaohu②**
(*School of Information Engineering, Wuhan University of Technology, Wuhan 430070, P.R. China)
(**School of Mechatronics Engineering and Automation, Shanghai University, Shanghai 200072, P.R. China)

Abstract

To study the effect of guide vane outlet angle on pump performance and impeller radial force in an axial-flow heart pump, guide vane outlet angle β_4 is considered to be 20°, 15°, 10°, 5° and 3° respectively. Based on ANSYS Fluent, numerical results of pump head and efficiency are validated by experiment results, in which Xanthan gum solutions are used with concentration of 0.06 wt.% as working fluid. Then, the effects of β_4 on pump performance and impeller radial force are discussed, the errors of head and efficiency between test and simulation are within 5%. The results also indicate that the pump performance and efficiency are much better than those of other angles when guide vane outlet angle β_4 is 10°, and the maximum variations in head and efficiency are 1.9% and 2.2%, respectively. With β_4 increasing, the pulsation of radial force decreases firstly and then increases, when β_4 is 10°, the minimum pulsation is 0.0392N, which is about 80% of the maximum pulsation amplitude.

Key words: heart pump, pump performance, guide vane outlet angle, radial force, rotor-stator interaction

0 Introduction

Heart pump is a mini-pump that can completely or partially replace heart function and maintain normal body blood circulation. It plays an important role in the treatment of cardiovascular disease and can significantly improve survival rate and quality of life of patients with severe congestive heart failure[1]. The guide vane can transfer the kinetic energy into pressure energy and smooth the flow distribution. Therefore, the guide vane is an important flow part in heart pumps. There are many researches about the influence of guide vanes on performance of the axial and mixed flow pumps[2,3]. But, at present, research of guide vanes on heart pump is very little, especially about how the guide vane can further reduce the radial force on an impeller. In practical work, a guide vane brings blood to artery or heart, which means its stability of blade, shaft and bearings is very important. So, radial forces deserve deep study. The radical force of impeller was experimentally researched by Okamoto[4], and he found the pressure fluctuations on the impeller was the main reason why there were many extra frequency components. Cheng[5] simulated a water jet pump and the calculation results agreed with the experimental data well, which proved that the validity of CFD model used in radial forces was trusted. Kruger[6] analyzed a vertical mixed pump by CFD, he found the vortexes distribution near pump inlet and radial force had a good agreement with experiment results. Adkins[7] predicted the radial force on the impeller theoretically, he also found that pressure affected the shroud of the impeller and produced radial force in the end. However, there is no relative study about the effect of guide vane outlet angle on impeller radial force in an axial-flow heart pump.

In the article, an axial-flow heart pump with 5 different guide vane outlet angles on the radial force is discussed intensively by both experimental and numerical methods, some meaningful conclusions are drawn.

1 Model test rig

In order to verify the simulation results, an experiment system of the research pump was established in Shanghai University. The schematic arrangements of

① Supported by the National Natural Science Foundation of China (No. 51574161) and the Education Science Project of Young and Middle-aged Teachers of Universities in Fujian Province (No. JZ160396).
② To whom correspondence should be addressed. E-mail: sangxh7@qq.com
Received on May 8, 2017

the test rig facilities are shown in Fig. 1. The motor is able to drive the pump with the designed rotation speed of 5000r/min. Two pressure transmitters are installed in the test loop to measure the inlet and outlet pressure respectively. And the measurement errors of the two pressure transmitters are both 0.1%. A gate valve is installed near the outlet of the loop to adjust the flow rate of the pump. A turbine flow meter is mounted behind the pressure transmitter near the gate valve to measure the volumetric flow rate of the pump. And the uncertainty of the magnetic flow meter is 0.1%. Besides, the pump head can be obtained by the pressure differential between the pressure of pressure port 1 and pressure port 2, a water column method is used and two glass tubes are respectively connected with the two pressure holes through a latex pipe, when the pump is working, the two glass tubes will arise a height difference, which can be converted into the pump head.

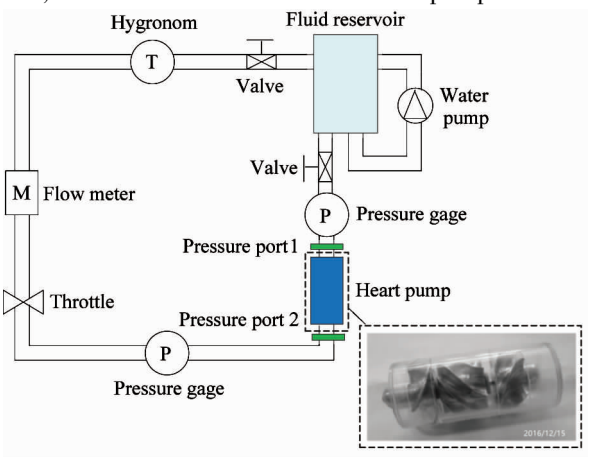

Fig. 1 The sketch of test rig

At last, aqueous Xanthan gum is a non-Newtonian fluid which displays remarkable shear thinning behavior and can be used as a blood analog fluid. Fig. 2 gives the Xanthan gum solution with different concentration. As shown in Fig. 3, the experimental results show that, compared with the Young and Kenneth[8] experiment date, at 37°C, Xanthan gum solutions with concentration of 0.06 wt.% will match human blood best in rheological properties[9-11].

Fig. 2 Xanthan gum solution for experiment

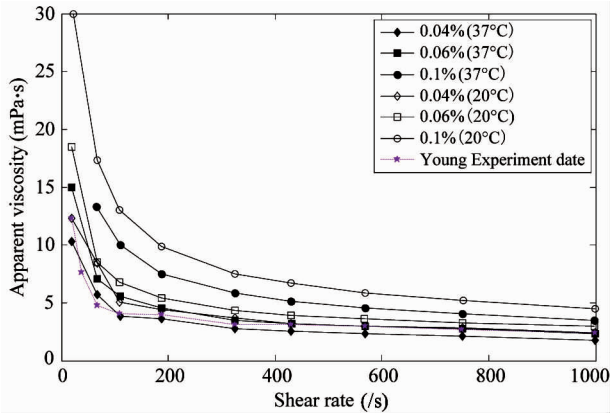

Fig. 3 Curves of apparent viscosity versus shear rate with different concentration

2 Numerical simulation

2.1 Research model

Parameters of the heart pump at the design operational condition are as follow: Flow rate $Q_d = 5$ l/min, nominal head $H = 120$mmHg, rotational speed $n = 5000$r/min and the rotational frequency of rotor $f = n/60 = 83.33$Hz. As shown in Fig. 4, the pump assembly mainly includes blade, guide vane, inlet pipe, outlet pipe, magnetic loop, motor stator, position sensor, pump shell and wire, etc[12]. The main geometric parameters of the test pump are listed in Table 1.

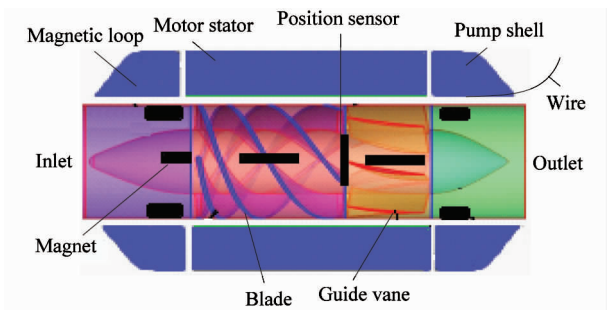

Fig. 4 Cross section of test pump

The three dimensional physical model of the hydraulic turbine is shown in Fig. 5, the lengths of outlet pipe and inlet pipe are extended to 3 times the pipe diameter to increase the simulation accurately[13].

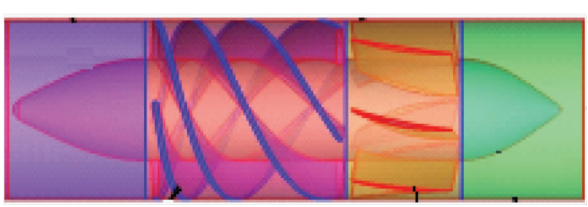

Fig. 5 Computational domain of the pump

Table 1 Main geometric parameters of test pump

Component	Sign	Value
Impeller and guide vane diameter	D(mm)	18
Impeller length	L_1(mm)	22
Guide vane length	L_2(mm)	15
Impeller thickness	ζ_1(mm)	0.5
Guide vane thickness	ζ_2(mm)	0.5
Blade number	Z_1	5
Guide vane number	Z_2	9
Impeller inlet angle	β_1(°)	18
Impeller outlet angle	β_2(°)	22
Guide vane inlet angle	β_3(°)	8
Guide vane outlet angle	β_4(°)	20°,15°, 0°,5°,3°
Rotational speed	n(r/min)	5000
Flow rate	Q(l/min)	5 – 7

As shown in Fig. 6, the outlet angle of the guide vane is designed to be 20°, 15°, 10°, 5° and 3°, respectively.

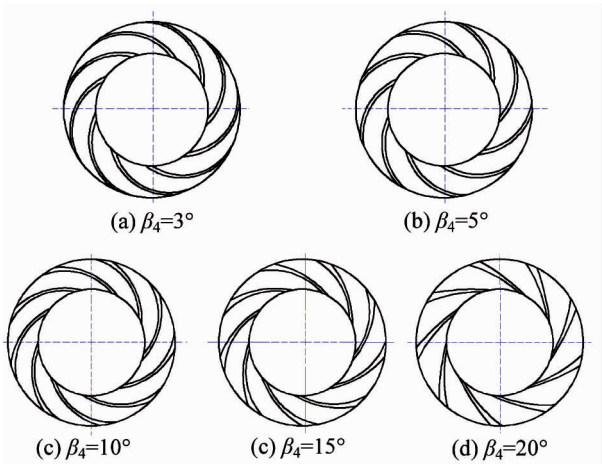

Fig. 6 Guide vane with different outlet angles

2.2 Grid formation

The grid is generated using a geometry preprocessor of the ICEM program. As the trailing edges of blades and diffuser are all quite thin, the size of grids can't be uniform. To form dense grids near the blades and diffuser trailing edge, a densification technique is utilized in some local blades and diffuser portion. As shown in Fig. 7, the mesh consists of a hybrid grid with prismatic and Hex-core cells.

2.3 Boundary conditions

Blood is a non-Newtonian fluid which displays remarkable shear thinning behavior,[14,15] when the shear rate is more than $100s^{-1}$, the human blood apparent viscosity becomes a constant value about 3.4 – 4.0 mPa · s,

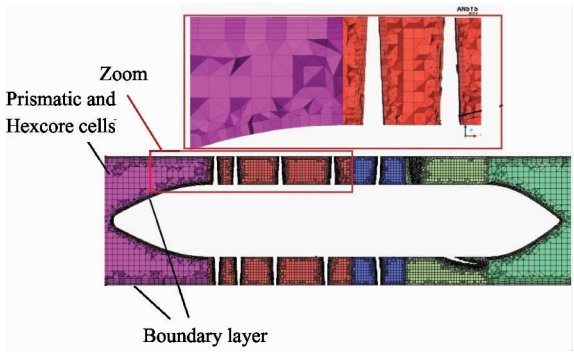

Fig. 7 Cross section of mesh

which means blood can be seen as Newtonian fluid[16,17], in the simulation, the viscosity and density are $\mu = 3.6$mPa · s and $\rho = 1055$ kg/m^3 respectively.

Inlet and outlet boundary conditions: velocity inlet is selected and 'outflow' is set as outlet.

Wall boundary condition: no slip condition is enforced on wall surface and enhanced wall function is applied to adjacent region, the near wall y^+ value should be less than 5. This study utilizes the ANSYS Fluent 17 commercial code to solve the RNG $k-\varepsilon$ equations for the unsteady flow in the computational domain. The SIMPLEC algorithm and second order implicit transient formulation are selected to solve pressure-velocity coupling for steady and unsteady simulation respectively. In addition, interfaces between impeller and other parts are set to be 'sliding mesh model (SMM)' while other interfaces remain to be 'General connection'. Time-step for unsteady simulations is given $1.1261e^{-3}$s, which namely means the impeller rotates for 1 degree during 5 time-step. Convergence precision of residuals is 10^{-4}.

2.4 Validation of grid independence

In order to check the influence of the grid on the results, 5 different type girds are validated, the results are shown in Table 2 and Fig. 8. It indicates that the pump head trends to rising along with the grids increased and tends to be smooth. Given the time cost for

Table 2 Grid independence analysis ($\times 10^6$)

Type	First stage	Guide vane	In & out	Amount
1	1.01	0.42	0.23	1.66
2	1.12	0.52	0.32	1.96
3	1.25	0.66	0.42	2.33
4	1.32	0.72	0.48	2.52
5	2.28	0.8	0.63	3.71
6	3.15	0.85	0.75	4.75

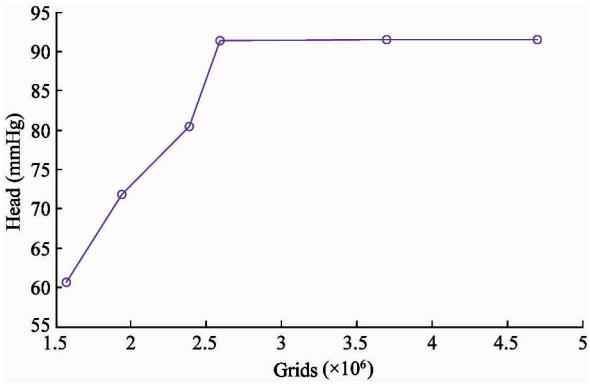

Fig. 8 Grid independence analysis

calculation considered, Type 4 is selected for calculation in the end. The mesh in the whole computational zones has 2 520 000 grids.

3 Prediction algorithm

Pump head is an important parameter of the heart pump, in medicine, differential pressure is used to indicate the head, its unit is mmHg, 100mmHg is equal to 1.38m head. Normal height is 1.5 – 2.0m, while heart is about 3/4 of the human body, that means 1.5m water column can basically meet the body's physiological pressure requirements. Under the premise of providing appropriate pressure difference, heart pumps also require adequate flow to meet the requirements of human blood perfusion, generally, it should meet 5 – 7 L/min condition.

According to Bernoulli equation:

$$\frac{V_{in}^2}{2g} + \frac{p_{in}}{\rho g} + \frac{H}{\rho g} + z_{in} = \frac{V_{out}^2}{2g} + \frac{p_{out}}{\rho g} + z_{out} \tag{1}$$

where, V_{in} is the velocity of the inlet (m/s), V_{out} is the velocity of the outlet (m/s), p_{in} is the pressure of inlet (Pa), p_{out} is the pressure of outlet (Pa), z_{in} is the height of inlet (m), z_{out} is the height of outlet (m), and H is the pump head (Pa).

$$\Delta H = \frac{p_{out} - p_{in}}{\rho g} + (z_{out} - z_{in}) \tag{2}$$

where ΔH (m) is the difference in height of pressure port 1 and pressure port 2.

Because pipe diameter $D_{in} = D_{out}$,

$$V_{in} = V_{out} \tag{3}$$

Simultaneous Eqs(1) – (3), the pump head can be deduced:

$$H = \rho g \Delta H \tag{4}$$

The efficiency of heart pump can be defined by

$$\eta = \frac{\rho g q H}{M\omega} \tag{5}$$

where, Q denotes the flow rate, ω denotes the angular velocity of impeller, and M denotes the moment of water on rotation axis.

In order to compare the experimental and numerical pump performance, the prediction error is defined by

$$e = \frac{H_{Exp} - H}{H_{Exp}} \times 100\% \tag{6}$$

where, e is the head prediction error, H_{Exp} is the experimental head of test pump, and H is the head of numerical model.

In CFD calculation, the radical can be computed[18] as

$$F_y = \iint_{A_2} V_x \rho V_r \mathrm{d}A - \iint_{A_1} V_x \rho V_r \mathrm{d}A - \rho \frac{\partial}{\partial t} \int_{V_T} \mathrm{d}QV_x - \iint_{A2} \cos(\theta + \omega t) p(r_2, \theta) \mathrm{d}A \tag{7}$$

$$F_y = \iint_{A_2} V_y \rho V_r \mathrm{d}A - \iint_{A_1} V_y \rho V_r \mathrm{d}A - \rho \frac{\partial}{\partial t} \int_{V_T} \mathrm{d}QV_y - \iint_{A_2} \cos(\theta + \omega t) p(r_2, \theta) \mathrm{d}A \tag{8}$$

$$F = \sqrt{F_x^2 + F_y^2} \tag{9}$$

where, F is the resultant force of radial force, A_1 and A_2 are the area of the impeller inlet and outlet, V_{T} is the radial velocity of a fluid particle at one point of impeller, V_x and V_y are the component velocity at x and y direction, θ is the initial angular velocity of fluid particle, and ρ is the fluid density.

$\iint_{A_2} V_x \rho V_r \mathrm{d}A - \iint_{A_1} V_x \rho V_r \mathrm{d}A$ and $\iint_{A_2} V_y \rho V_r \mathrm{d}A - \iint_{A_1} V_y \rho V_r \mathrm{d}A$ denote the momentum static flow of the impeller, $\rho \frac{\partial}{\partial t} \int_{V_T} \mathrm{d}QV_x$ and $\rho \frac{\partial}{\partial t} \int_{V_T} \mathrm{d}QV_y$ indicate the change rate of impeller internal momentum with time, $\iint_{A_2} \cos(\theta + \omega t) p(r_2, \theta) \mathrm{d}A$ is the pressure of outlet at y direction, thus there is no term of inlet pressure.

4 Selection of turbulence model

Turbulence model selection is a crucial part for numerical simulation, because inappropriate turbulence model always leads to high calculation error. Fig. 9 gives the curves of numerical and experimental results and the Standard $k-\varepsilon$, RNG $k-\varepsilon$, $k-\omega$, turbulence models have been used to simulate the inner flow of the pump. As shown in Fig. 9, numerical performance curves are in good agreement with experimental results. For the range of $Q/Q_{\mathrm{d}} = 0.4 - 1.2$, RNG $k-\varepsilon$ turbulence model is closest to the experiment data. So the RNG $k-\varepsilon$ turbulence model is adopted to perform simulations in this paper.

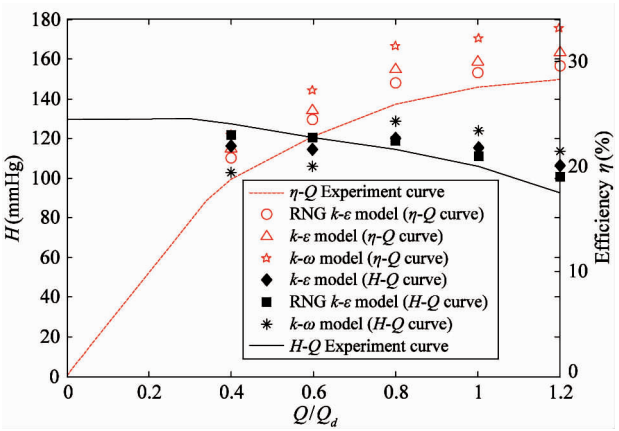

Fig. 9 Comparison of different numerical model

5 Results and discussions

5.1 Influence of guide vane outlet angle on the pump performance

Fig. 10(a) – (e) gives the pump performance of numerical and experimental results with different guide outlet angle β_4. Q represents the actual flow, Q_d is the design flow. As shown in the figures, all numerical performance curves are in good agreement with experimental results. For the value of $Q/Q_d = 1$, the errors of efficiency and head between test and simulation are within 5%. The results also indicate that when the guide vane outlet angle β_4 is 10°, the pump performance and efficiency are better than other angles, the maximum variations in head and efficiency are 1.9% and 2.2%, respectively.

The number is a little bigger than the experimental result. While, the numerical head is less than experimental dates as $Q/Q_d = 0.4$, the reason is that the inverse flow happens at a small flow rate, which is caused by unsteady turbulent flow. For the range of other Q/Q_d, the deviation is influenced by mechanical

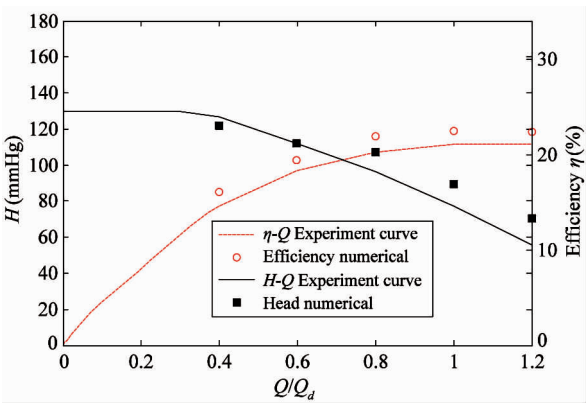

(a) $\beta_4 = 3°$

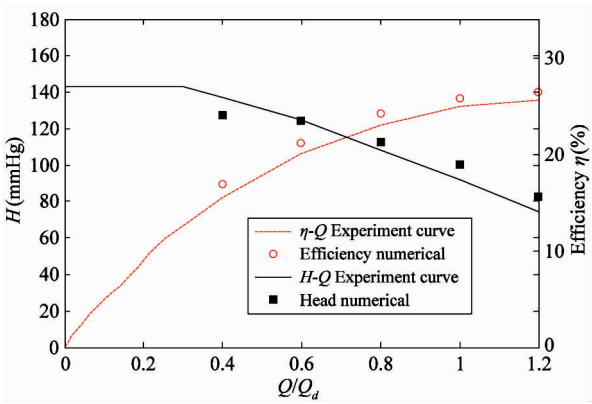

(b) $\beta_4 = 5°$

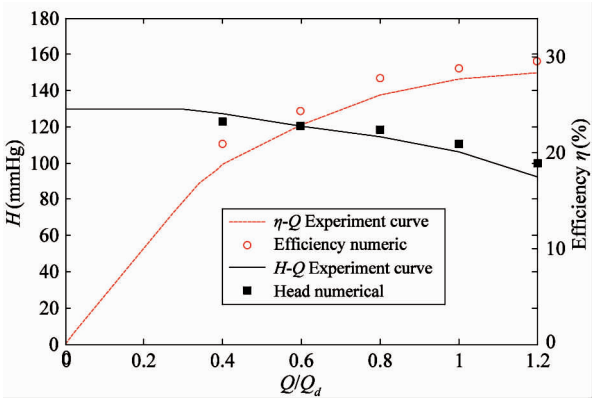

(c) $\beta_4 = 10°$

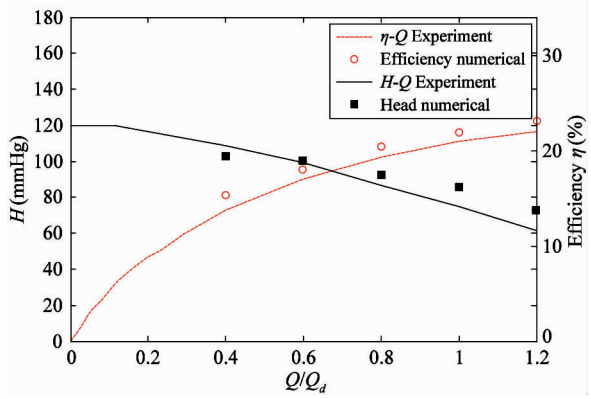

(d) $\beta_4 = 15°$

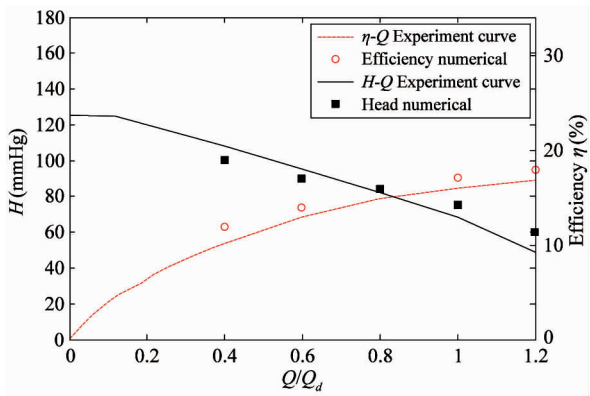

(e) $\beta_4 = 20°$

Fig. 10 Pump performance of numerical and test results under different guide vane angles

loss. The comparison between numerical and experimental results proves that the CFD method could predict the pump performance with acceptable accuracy.

Fig. 11 shows the head and efficiency changes of the pump with the decrease of β_4. With β_4 decreasing, the head and efficiency of the pump increase at first and then decrease dramatically, the head and efficiency of the pump are best when the guide vane outlet angle β_4 is 10°, the maximum pump head and efficiency are 110mmHg and 29%.

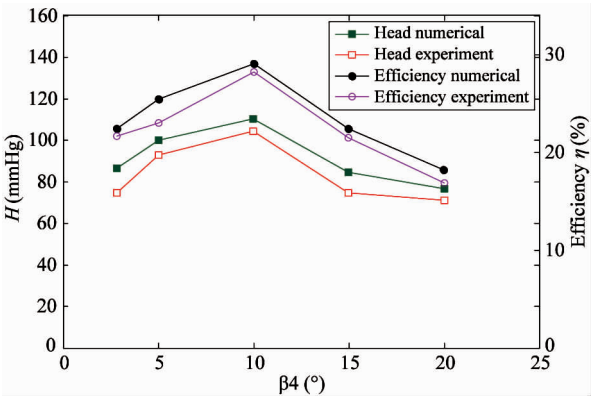

Fig. 11 Pump performance with guide vane outlet angle changes

Changes of pump performance can be also reflected by the changes of inner flow field. In order to see the reasons, the velocity streamlines at the guide vanes are shown in Fig. 12. The recirculation at $\beta_4 = 5°$ spreads over the one-third height of suction-side of guide vane, and expands gradually with increased β_4, while it disappears at $\beta_4 = 10°$. When β_4 is 15° and 20°, the recirculation takes over almost the whole guide vane, which causes more kinetic energy loss. Obviously, the expanded recirculation causes bad pump performance.

5.2 Analysis for time and frequency domain characteristics of radial force

Fig. 13(a) – (e) gives the time domain curves of radial force with different β_4. As it can be seen from the graph, all the pulsations of the radial forces are periodic, the trend of radial force fluctuation is more consistent. Within a rotation period, the radial force pulsation generally appears periodically for 5 times, which equals the impeller number Z_1 due to the rotor-stator interaction between the impeller and the guide vane obviously. When $\beta_4 = 3°$, the peak-valley structure firstly appears at 0.003s, with β_4 increasing, the time of peak-valley structure moves forward, which shows the change of β_4 has an impact on the pulsation of radial force and the phase of radial force fluctuation waveform.

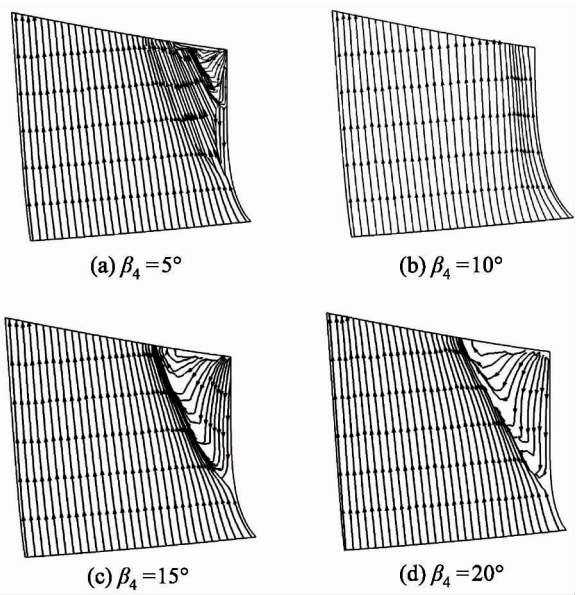

Fig. 12 Streamline distribution chart in suction-side of guide vane

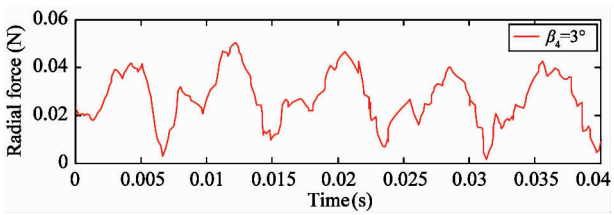

(a) $\beta_4 = 3°$

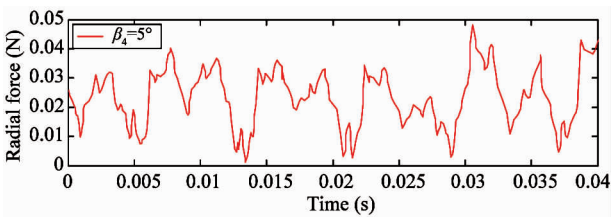

(b) $\beta_4 = 5°$

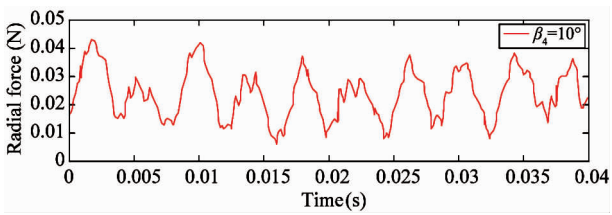

(c) $\beta_4 = 10°$

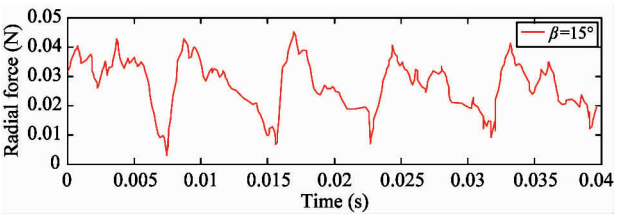

(d) $\beta_4 = 15°$

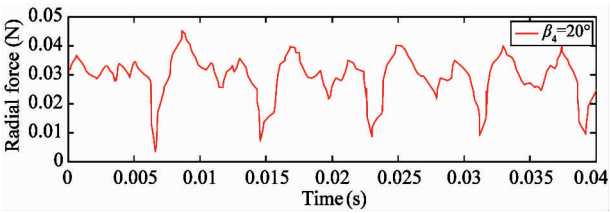

(e) $\beta_4 = 20°$

Fig. 13 Time domain curves of radial force pulsation with different β_4

In order to analyze the characteristics of radial force fluctuation, Table 3 displays specific data for maximum radial force, minimum radial force and peak-valley pulsation value with different β_4. When β_4 falls from 20° to 3°, the maximum radial force is 0.0501N, which is at 3°; the minimum radial force is 0.0432N when β_4 is 10°. Meanwhile, the minimum peak-valley pulsation value appears at 10° too, which is about 80% of the maximum value from 0.0392N to 0.0489N.

Table 3 Radial force at different β_4

β_4 (°)	Radial force (N)		
	Max value	Min value	Peak-valley pulsation value
20	0.0451	0.0026	0.0425
15	0.0446	0.0028	0.0418
10	0.0432	0.004	0.0392
5	0.0481	0.0006	0.0475
3	0.0501	0.0012	0.0489

The direction and magnitude of transient radial forces are applied on impeller change with impeller rotation all the time, the transient dynamic forces data could be calculated through the unsteady CFD simulation. The rotary speed of the rotor is 5000 r/min that means the rotational frequency of rotor is 83.33Hz, blade passing frequency is 416.67Hz.

A fast Fourier transform (FFT) then is applied to obtain the detailed radial force distribution. Fig. 14 gives the radial force in frequency spectrum of different β_4. It can be seen, the radial force fluctuation is mainly concentrated in the low frequency region and the peak value of the pulsation occurs mostly at the harmonic frequency. With β_4 increasing, the dominant frequency of radial force increases first and then decreases. When β_4 are 3° and 20°, the dominant frequency of radial force pulsation is all 416.67Hz, which equals the blade passing frequency. When β_4 is 10°, the dominant frequency is 833.33Hz, which is 10 times of the rotational frequency and twice the blade passing frequency.

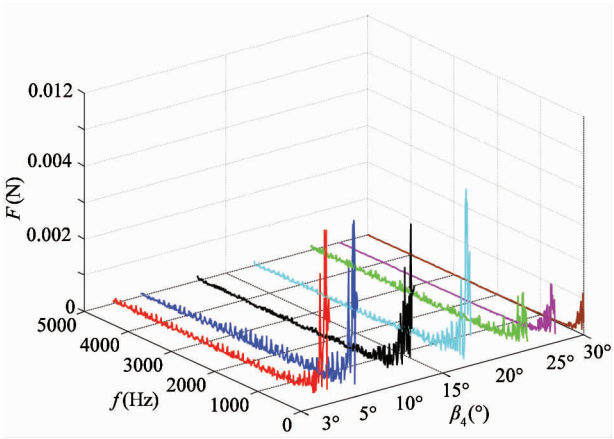

Fig. 14 Radial force in frequency domain with different β_4

Eisenmann[19] pointed out that the rotation of impeller blades was the dominant factor of radial force fluctuation. When β_4 is 10°, the dominant frequency is 833.33Hz, the value is twice the blade passing frequency, which shows that the main factor of the radial force fluctuations is the interaction between impeller and guide vane. In a word, it is mainly due to the small gap between impeller and guide vane.

6 Conclusions

In the article, an axial-flow heart pump is used as the object of study. The computational and experimental analysis of the results could be summarized as follows.

With the guide vane outlet angle β_4 decreasing, the head and efficiency of the pump increase at first and then decrease dramatically, the head and efficiency of the pump are best when the guide vane outlet angle β_4 is 10°, the maximum pump head and efficiency are 110mmHg and 29%. The comparison between numerical and experimental results proves the CFD method could predict the pump performance with acceptable accuracy.

With β_4 increasing, the pulsation of radial force decreases firstly and then increases, when β_4 is 10°, the minimum pulsation is 0.0392 N, which is about 80% of the maximum pulsation amplitude. With the increase of β_4, the time of peak-valley structure moves forward, which shows the change of β_4 has an impact on the pulsation of radial force and the phase of radial force fluctuation waveform.

When β_4 is 3° and 20°, the dominant frequency of radial force pulsation is 416.67Hz, the value equals the blade passing frequency. When β_4 is 10°, the dominant frequency is 833.33Hz, which is 10 times of

the rotational frequency and twice the blade passing frequency, which is mainly due to the small gap between impeller and guide vane.

References

[1] Boehning F, Timms D L, Amaral F, et al. Evaluation of hydraulic radial forces on the impeller by the volute in a centrifugal rotary heart pump [J]. *Artificial Organs*, 2011, 35(8): 818-825

[2] Hu E F, Chen T, Wu D, et al. Experimental study of cavitation vibration and noise of guide vane mixed flow pump[J]. *Journal of Drainage and Irrigation Machinery Engineering*, 2013, 31(12): 1021-1024

[3] Bing H, Cao S, Tan L, et al. Effects of diffuser vane on mixed-flow pumps performance[J]. *Journal of Drainage and Irrigation Machinery Engineering*, 2012, 30(2): 125-130

[4] Guo S, Okamoto H. An experimental study on the fluid forces induced by rotor-stator interaction in a centrifugal pump[J]. *International Journal of Rotating Machinery*, 2003, 9(2): 135-144

[5] Cheng L, Esch B P M V, Liu C, et al. Radial force of water-jet propulsion mixed-flow pump [J]. *Journal of Drainage and Irrigation Machinery Engineering*, 2012, 30(6): 636-640

[6] Kruger S, Bouziad Y A, Maurer W. Pump sump CFD for vertical pump design[C]. In: Proceedings of the ASME Fluids Engineering Division Summer Conference, Colorado, USA, 2009. 191-198

[7] Adkins D R, Brennen C E. Analyses of hydrodynamic radial forces on centrifugal pump impellers[J]. *Journal of Fluids Engineering*, 1986, 110(1): 20-28

[8] Young I C, Kenneth R K. Effect of the non-Newtonian viscosity of blood on flows in a stenosed arterial vessel [J]. *Biorheology*, 1991, 28(3-4): 241

[9] Zhang G G, Zhang M Y, Zhu X R, et al. Experimental investigation of rheological properties of blood and Xanthan gum solutions as a blood analog fluid[J]. *Journal of Experiments in Fluid Mechanics*, 2007, 21(2): 21-24

[10] Yang WY, Zhang M Y, Zhang G G, et al. Hydrodynamics of non-Newtonian fluids in a centrifugal blood pump [J]. *Journal of Experiments in Fluid Mechanics*, 2008, 22(03): 60-63

[11] Miklosovic D S. An experimental evaluation of the non-Newtonian scaling effects in a rotodynamic left ventricular assist device:[Ph. D dissertation][D]. Columbus: The Ohio State University, 1999

[12] Akamatsu T, Tsukiya T. Development of a centrifugal heart pump with magnetically suspended impeller and the related fluid mechanical problems[J]. *Sadhana*, 1998, 23(5): 597-603

[13] Brennen C E. Hydrodynamics of Pumps[M]. Oxford: Concepts Nrec & Oxford University Press, 1994

[14] Chien S, Usami S, Dellenba R J, et al. Blood viscosity influence of erythrocyte aggregation[J]. *Science*, 1967, 157(3790): 829-831

[15] Chien S, Usami S, Dellenba R J, et al. Blood viscosity influence of erythrocyte deformation[J]. *Science*, 1967, 157(3790):827-829

[16] Huang C R, Fabisiak W. A rheological equation characterizing both the time dependent and the steady state viscosity of whole human blood[J]. *American Institute of Chemical Engineers-Symposium Series*, 1978, 74: 19-21

[17] Ng E Y K, Zhou W D. Non-Newtonian flow in a large mixed flow pump[J]. *International Journal of Computer Applications in Technology*, 2000, 13(6): 332-345

[18] Zhang M, Wang H, Tsukamoto H. Unsteady hydrodynamic forces due to rotor-stator interaction on a diffuser pump with identical number of vanes on the impeller and diffuser[J]. *ASME Journal of Fluids Engineering*, 2005, 127(4): 2020-2027

[19] Eisenmann R C. Machinery Malfunction Diagnosis and Correction: Vibration Analysis and Troubleshooting for the Process Industries[M]. London: Prentice Hall, 1998

Liu Fufei, bron in 1979. Now he is a Ph. D candidate in Wuhan University of Technology. He received his M. S degree from Jiangxi University of Science and Technology in 2009. His current research interests include fluid power transmission and control, optic fiber sensing.